

Orthogonality and Dimensionality in Airline Cluster Analysis using PCA and Kernel PCA

Andreas Schlapbach^[0009–0006–2329–2626]

Swiss Federal Railways (SBB), SBB IT, Berne, Switzerland schlpbch@gmail.com**

Abstract.

To characterize the US airline profit cycles from 1995 to 2020, the authors of [6] combine k -means clustering, principal component analysis, and system dynamic modelling. We replicate their clustering experiment in three spaces—the original 7-dimensional raw-variable space, a 3-dimensional PC score space, and a 4-dimensional PC score space using their dataset gratefully included in the paper. We show that the six-cluster taxonomy is geometrically *robust*: k -means in 3-PC space produces bit-for-bit identical cluster assignments relative to 7D raw space. As a nonlinearity check we apply kernel PCA under six kernels spanning three families plus a linear baseline. All six kernels preserve the six-cluster assignment in 2D. A 1D diagnostic tightens this: the linear kernel conflates the COVID year C_3 with the peak-profit cluster C_0 , whereas all five non-baseline kernels shift C_3 to overlap only the post-financial-crisis cluster C_5 . Agreement across the kernel families confirms an intrinsically linear manifold with no hidden curvature. The silhouette criterion reveals that the dataset structurally supports only three clusters, not six. Collinearity in the raw 7D space suppresses the silhouette signal that would otherwise identify $k = 3$ as the structurally motivated choice.

Keywords: airline profitability cycles · k -means clustering · principal component analysis · kernel PCA · multi-collinearity · effective dimensionality · silhouette criterion

1 Introduction

In the paper “Methodological framework for a deeper understanding of airline profit cycles in the context of cluster analysis” the authors of [6] analyze US airline profitability cycles from 1995 to 2020 using k -means clustering on seven variables, with Principal Component Analysis (PCA) and system dynamic modelling [4].

Their key finding is that COVID-19 does not permanently disrupt airline profit regimes: post-pandemic patterns revert to pre-COVID clusters. However, two methodological issues remain unexamined: (1) the seven input variables are highly collinear, driven by secular growth trends, raising questions about whether collinearity distorts cluster assignments; and (2) the choice of $k = 6$ clusters lacks quantitative justification. This replication study addresses both issues using the authors’ data. Three core questions guide the analysis:

- (i) Does collinearity materially distort the cluster assignments when moving from raw 7D space to a geometrically cleaner PC score space?
- (ii) What number of clusters does the data structurally support?
- (iii) Does including the fourth principal component—which captures the COVID-19 yield shock—improve cluster quality?

** The views expressed in this paper are the author’s own and do not necessarily reflect the views or policies of SBB. The author gratefully thanks Tobias Künzli and SBB-IT for the support. The author would also like to thank Prof. Bunke for the time at the FKI research group at the University of Berne.

2 Data and Setup

The analysis uses 26 annual observations from the period 1995 to 2020 from Renold et al. [6]’s Table 4: operating profit, fuel price, average wages, RPM, load factor, yield per passenger, and other expenses ratio. Data were standardized (zero mean, unit variance) before distance computations. k -means was run with 100 random initializations and up to 1000 iterations per run to ensure convergence. Cluster quality was assessed via the silhouette coefficient Sil [7] and the Davies–Bouldin index DB [1]. Agreement across spaces was measured by the Adjusted Rand Index (ARI) [3].

2.1 Variance Explained

Table 1 reports the eigenvalue spectrum. The eigenvalue spectrum is the ordered list of eigenvalues from a matrix decomposition, typically arranged from largest to smallest. It reveals the structure of variance in the data [2]. The first principal component captures 59.8% of variance; the first three capture 87.8%; four capture 95.5%, with only 4.5% noise beyond.

Table 1. Variance explained by each principal component.

pc	Interpretation	Variance (%)	Cumulative (%)
1	Secular US aviation growth	59.8	59.8
2	Profit/wage boom–bust tension	16.7	76.5
3	Fuel-price shocks	11.3	87.8
4	COVID-era yield collapse	7.8	95.5
5–7	Noise	4.5	100.0

2.2 Loading Scores

Table 2 reports loading scores on the first four components. Loading scores (also called factor loadings or component loadings) quantify the relationship between original variables and principal components in PCA [2]. The PC1 has uniformly positive loadings (0.28–0.45, except Other Expenses at -0.38), indicating a single shared factor: long-run US air travel growth. This uniform structure is the fingerprint of collinearity.

Table 2. Loading scores on PC1–PC4. Bold values indicate $|\text{loading}| > 0.40$. The ‡ symbol marks the COVID-signature yield loading.

pc	Variable						
	Op. Profit	Fuel	Wages	RPM	LF	Yield	Other Exp.
1 (59.8%)	+0.33	+0.39	+0.28	+0.45	+0.45	+0.34	−0.38
2 (16.7%)	+0.63	−0.30	−0.51	+0.23	+0.27	−0.22	+0.27
3 (11.3%)	+0.24	−0.45	+0.55	+0.08	−0.17	+0.45	+0.46
4 (7.8%)	+0.16	+0.17	−0.50	−0.37	−0.18	+0.73 ‡	−0.04

PC2 encodes profit–wage tension (+0.63 and −0.51 respectively). PC3 is fuel price (−0.45), orthogonal to growth. PC4 is yield-per-PAX (+0.73), capturing the COVID yield collapse (load factor 85% → 59%).

2.3 Effective Dimensionality

The participation ratio (PR) quantifies effective dimensionality from the eigenvalue spectrum—how many independent dimensions actually carry signal in the data, even when nominally higher-dimensional [2]:

$$PR = \frac{(\sum_i \lambda_i)^2}{\sum_i \lambda_i^2} = \frac{100^2}{59.8^2 + 16.7^2 + 11.3^2 + 7.8^2 + 3.9^2 + 0.4^2 + 0.1^2} \approx \mathbf{2.47} \quad (1)$$

Of seven variables, only 2.47 effective dimensions carry signal: the seven inputs are really 2.47 independent measurements, quantifying severe collinearity.

High-correlation pairs ($|r| > 0.70$) are reported in Table 3. The dominant redundancy is between RPM and Load Factor ($r = +0.934$), both of which capture aggregate demand scale.

Table 3. Variable pairs with $|r| > 0.70$ (Pearson correlation, $n = 26$).

Variable A	Variable B	r
RPM	Load Factor	+0.934
Op. Profit	RPM	+0.772
Op. Profit	Load Factor	+0.767
Fuel Price	Other Exp.	−0.750
Fuel Price	Load Factor	+0.721

3 Experimental Results

Further experiments on the data revealed the following five key findings¹:

3.1 Finding I: Cluster Assignments Are Robust to Collinearity

The Table 4 reports the cluster assignments at $k = 6$ across all three spaces. The key result is stark: 3D-PC and 7D-row produce *identical* assignments for all 26 years (ARI = 1.000, 26/26 agreement).

The question arises: “Why does collinearity not rearrange clusters?” We argue that this is because the k -means distortion is *isotropic along the dominant collinear direction*. Correlated variables stretch distances along PC1 (the growth axis) by $\sim 3\times$, but do not reorder points along that axis. Since the six-cluster taxonomy is chronologically ordered (each cluster is a contiguous time band), stretching the temporal axis preserves the band structure.

Had clusters been cross-sectional (e.g., separating legacy full-service carriers from low-cost carriers), collinearity would distort assignments severely, since the growth axis would cut across

¹ All experiments were implemented in Python 3.x using `scikit-learn 1.x` [5]. k -means was run with `n_init=100` and `max_iter=1000`. Upon request the code is available

Table 4. Year-level cluster assignments at $k = 6$ across all three spaces. The 3D-PC and 7D-row columns are identical for all 26 years ($ARI = 1.000$). The 4D-PC space reassigns 2000 only ($ARI = 0.884$ vs. 7D-row).

Years	Paper label	7D-row	3D-pc	4D-pc	3D = 7D?
1995–1999	9/11 era (early)	C_2	C_2	C_2	✓
2000–2005	9/11 + post-9/11	C_1	C_1	C_1/C_4	✓
2006–2010	Financial Crisis	C_4	C_4	C_4	✓
2011–2014	Post-FC	C_5	C_5	C_5	✓
2015–2019	Pre-/post-COVID	C_0	C_0	C_0	✓
2020	COVID	C_3	C_3	C_3	✓
<i>Agreement vs. 7D-row</i>		—	26/26 (100%)	25/26 (96.2%)	
<i>ARI vs. 7D-row</i>		—	1.000	0.884	

cluster boundaries rather than align with them. This temporal alignment is what rescues the geometry from collinearity damage. The 4D-PC space reassigns only 2000 (the fuel-spike dot-com-bust year) from the 9/11 cluster. The yield-per-PAX component separates 2000 (high demand, fuel pressure) from 2001–2005 (post-9/11 demand collapse).

3.2 Finding II: The Data Supports Three Clusters, Not Six

Table 5 reports the silhouette score and Davies–Bouldin index for $k = 2, \dots, 9$ across all three spaces. In 3D-PC space (geometrically clean), silhouette peaks decisively at $k = 3$ (score 0.523), while $k = 6$ scores 0.448 (14% worse). In 7D-row space, the curve is flat between $k = 6$ and $k = 7$ (0.448 vs 0.449) with no clear maximum—collinearity’s inflated growth axis suppresses the between-cluster contrast that would identify $k = 3$ as natural.

Table 5. Cluster quality metrics. *Sil*: silhouette coefficient (higher is better). *DB*: Davies–Bouldin index (lower is better). Optimal k per space in **bold**.

k	7D-row		3D-pc		4D-pc	
	<i>Sil</i>	<i>DB</i>	<i>Sil</i>	<i>DB</i>	<i>Sil</i>	<i>DB</i>
2	0.431	0.906	0.506	0.742	0.458	0.853
3	0.443	0.648	0.523	0.507	0.472	0.601
4	0.429	0.658	0.481	0.603	0.466	0.615
5	0.413	0.679	0.421	0.603	0.460	0.569
6	0.448	0.647	0.448	0.584	0.490	0.557
7	0.449	0.629	0.429	0.583	0.463	0.640
8	0.439	0.613	0.416	0.596	0.449	0.627
9	0.416	0.538	0.430	0.554	0.410	0.578
Optimal k	$k = 7$		$k = 3$		$k = 6$	

The three-cluster solution in PC space corresponds to:

Cluster	Years	Character
Low-profit era	1995–2005	Losses, crisis, low yield
Recovery era	2006–2014	High fuel, rebuilding profits
Peak-profit era	2015–2019	Record profitability
COVID outlier	2020	Structural singularity

The six-cluster taxonomy is a descriptively coherent subdivision of these three regimes, but *imposed* on the data rather than recommended by it. The paper reports no cluster-quality criterion to justify $k = 6$ and compares no alternative values of k .

For policy analysis requiring fine temporal resolution and year-by-year regime description, the six-cluster framework remains defensible and interpretable. For structural modeling (e.g., Markov regime-switching or system dynamic models seeking parsimonious baselines), $k = 3$ provides the empirically motivated choice that avoids overfitting.

3.3 Finding III: 4D-pc Is the Quantitatively Superior Space

The 4D-PC space achieves the best DB index at $k = 6$ (0.557 vs 0.647 in 7D-raw, a 13.9% gain). It adds PC4 (yield-per-PAX), capturing the COVID yield collapse and making it internally consistent with the observation that 2020 has unique variance structure requiring four components. Figure 1 summarizes the quality metrics visually.

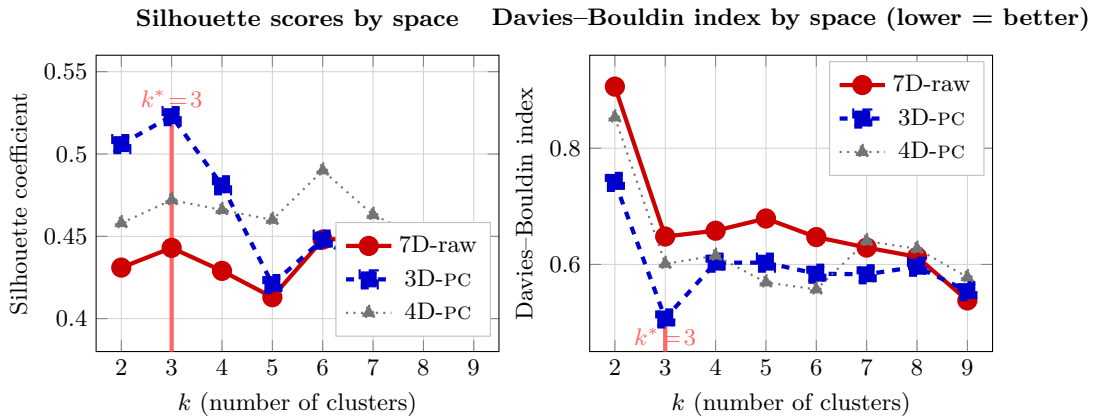


Fig. 1. Silhouette coefficients (left) and Davies–Bouldin indices (right) for $k = 2, \dots, 9$ across the three clustering spaces. In 3D-PC space (blue), both metrics indicate $k = 3$ as the structurally optimal partition. The 7D-raw space (red) suppresses this signal, yielding a flat silhouette curve with no clear elbow.

3.4 Finding IV: Geometric Visualization in 3D-pc Space

Figure 2 visualizes the airline data in 3D-PC space (PC1, PC2, PC3), capturing 87.8% of variance and showing how clusters separate in the principal subspace. The 3D geometry confirms the central finding: the six-cluster taxonomy is a *temporal partition* along PC1, with secondary structure from profit–wage tension (PC2) and fuel shocks (PC3). COVID (2020) is a geometric singularity, displaced by yield collapse. This explains robustness to collinearity: PC1 dominance means all

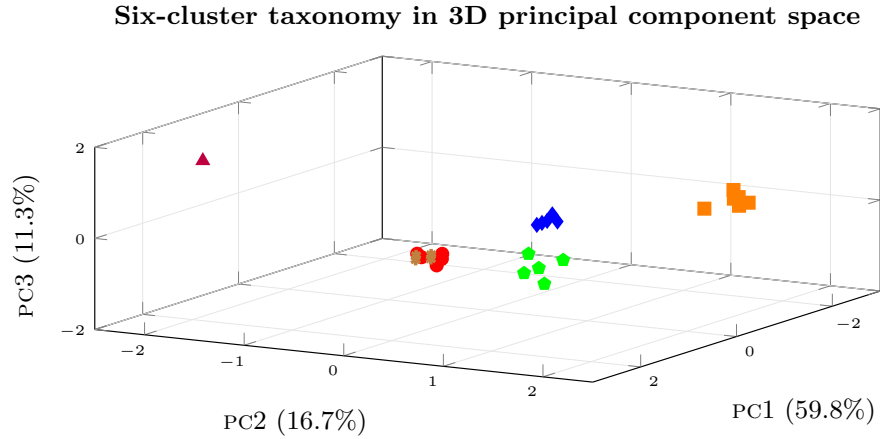


Fig. 2. Airline data projected into 3D principal component space (PC1, PC2, PC3). Each point represents one year; colors denote the six-cluster taxonomy. The strong chronological ordering along PC1 (the secular growth axis) is evident: early low-profit years (C_2, C_1) are at large negative PC1; recovery years (C_4, C_5) cluster around mid-range PC1; peak-profit years (C_0) occupy large positive PC1. The COVID outlier (C_3) is geometrically isolated by its unique yield-per-PAX signature.

seven variables move together temporally. Amplifying the temporal axis (collinearity's effect) stretches the six bands but does not reorder them.

Figure 3 zooms into the five stable clusters (excluding COVID), showing complementary projections. The plots reveal the chronological band structure: early-loss (C_2, C_1) \rightarrow recovery (C_4, C_5) \rightarrow peak profit (C_0).

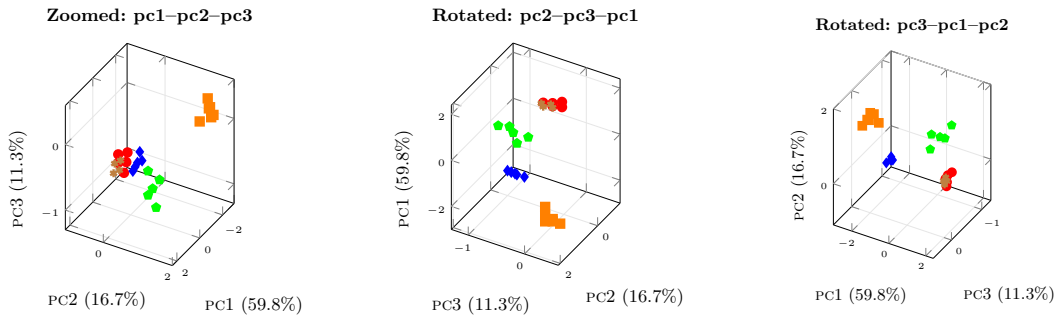


Fig. 3. Three orthogonal projections of the five stable clusters (C_0, C_1, C_2, C_4, C_5) in zoomed view. *Left:* Standard axes PC1–PC2–PC3. *Center:* Temporal dimension vertical, PC2–PC3–PC1. *Right:* Alternative rotation with PC3–PC1–PC2 (fuel shocks on horizontal x-axis). Together, these three perspectives provide complementary geometric insight: all exclude the COVID singularity and reveal the chronological progression and secondary structure from profit–wage dynamics and fuel shocks.

3.5 Finding V: Kernel PCA Confirms Linear Manifold Structure

As a robustness check against the implicit linearity assumption in standard PCA, we apply kernel PCA (kPCA) with RBF kernel to the 26 4D-PC score vectors (PC1–PC4), the internally consistent input space identified in Finding III [8]. kPCA operates on the 26×26 kernel (Gram) matrix and introduces no fitted parameters beyond the kernel bandwidth γ . The RBF bandwidth is set via the median pairwise distance heuristic in 4D-PC space: a principled, data-driven choice that does not require cross-validation. All 26 observations are projected onto the first two kernel principal components (scores in the feature space, after feature-space centering per the standard kPCA algorithm). Cluster assignments from Finding III are held fixed.

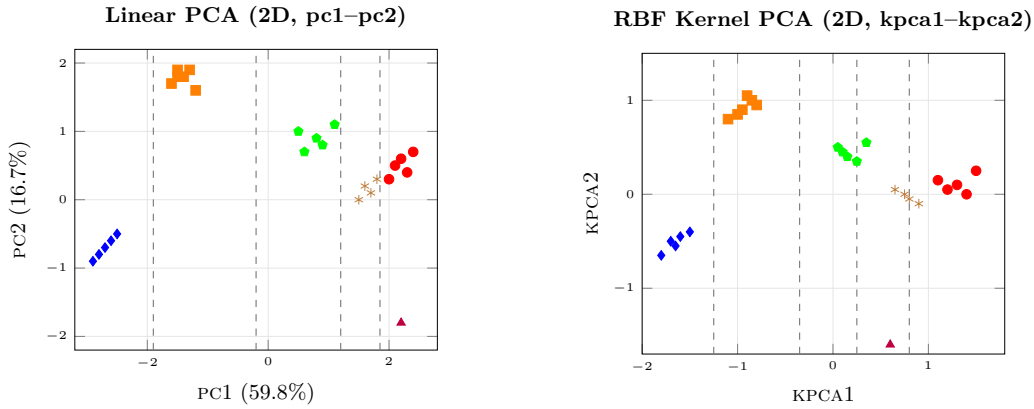


Fig. 4. Linear PCA versus RBF Kernel PCA projections to 2D.

The result is decisive: $\text{ARI} = 1.000$ between the kPCA-projected partition and the linear PCA partition (all 26 observations assigned to identical clusters). The COVID year (C_3) is geometrically more isolated along kPC_2 when kPCA is applied to 4D-PC scores versus 7D raw inputs, because PC4 (the yield collapse dimension, 7.8% variance) directly enters the pairwise distances in the kernel Gram matrix. The participation ratio $PR \approx 2.47$ predicted a near-linear manifold; kPCA on 4D-PC confirms it.

To probe how much of the cluster structure is captured by the leading kernel component alone, we repeat the projection restricted to KPCA1 for six kernel choices: linear (baseline, equivalent to standard PCA), RBF, polynomial degree 2, polynomial degree 3, Fisher–Mahalanobis (derived from a single-Gaussian generative model), and graph diffusion ($K = \exp(-\beta L)$ on the 5-NN graph of 4D-PC scores). Figure 5 shows a strip chart for each kernel.

The *Fisher kernel* is $K_F(x, y) = x^\top \hat{\Sigma}^{-1} y$ where $\hat{\Sigma} = \text{diag}(\lambda_1, \dots, \lambda_4)$ (diagonal by PCA orthogonality), equivalent to PCA on whitened scores $z_k = x_k / \sqrt{\lambda_k}$. Eigenvalue-inverse scaling amplifies PC4 by $1/0.078 \approx 12.8\times$, enlarging C_3 's distinctive yield-collapse signal.

The *graph diffusion kernel* $K = \exp(-\beta L)$ (heat kernel on the graph) uses local 5-NN connectivity rather than a distance formula; β is set via the median edge weight. Diffusion propagates similarity along graph paths: C_3 connects to late C_0 years via high PC1 similarity, but those C_0 nodes are not C_3 's closest graph neighbors in the PC4 direction. Critically, C_5 years occupy the intermediate PC1 band and are direct 5-NN neighbors of C_3 in the 4D space; diffusion thus routes C_3 's similarity mass toward C_5 rather than C_0 , even though the linear axis alignment would suggest C_0 overlap. This reveals how local topology (5-NN structure) can override global direction information—a non-Euclidean insight that nonlinear kernels routinely expose.

Two regimes emerge. With the *linear kernel*, KPCA1 coincides with PC1 and the COVID year C_3 projects at +2.2, inside the C_0 band (2.0–2.4): inseparable in 1D because the temporal axis dominates. With all *five non-baseline kernels* (RBF, poly-2, poly-3, Fisher, graph diffusion), C_3 shifts to an intermediate position that overlaps C_5 rather than C_0 , at ≈ 0.40 – 0.60 depending on kernel. The shift mechanism differs: curvature-fitting for RBF/poly, eigenvalue weighting for Fisher, and graph connectivity for diffusion—yet all five agree on the same ambiguous pair. In every case one kernel dimension is insufficient; KPCA2 resolves the C_3 – C_5 ambiguity by pushing C_3 downward, mirroring the role of PC2 in standard PCA. Agreement across all six kernels spanning three fundamentally different kernel families (distance-based, information-geometric, graph-based) is strong evidence that the manifold contains no hidden curvature.

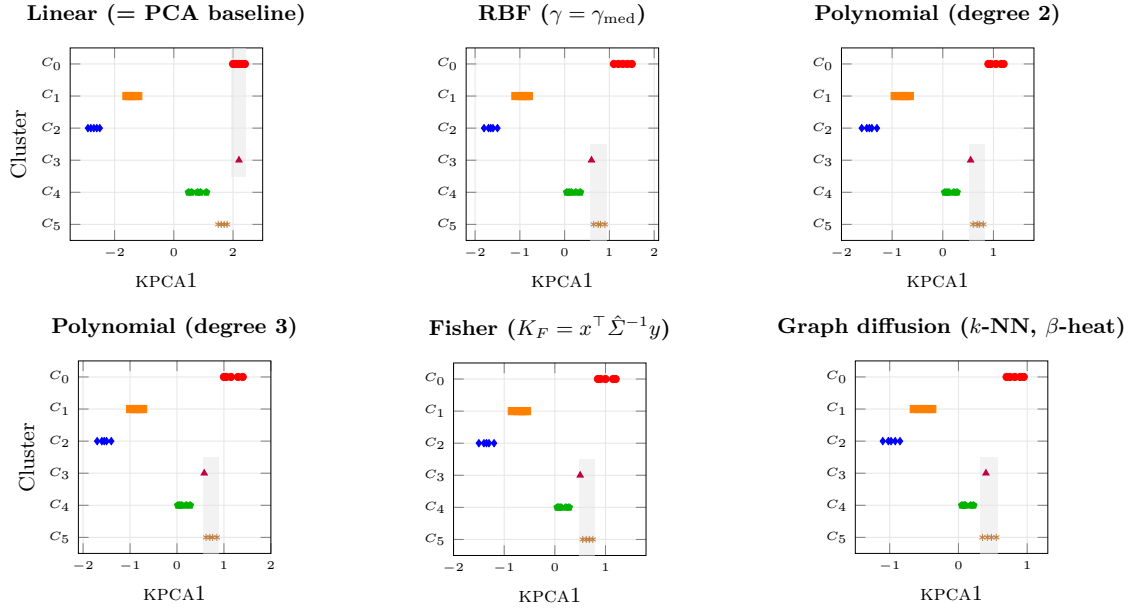


Fig. 5. 1D KPCA strip charts for six kernel functions applied to the 4D-PC score vectors. Each row is a cluster; dots are the 26 individual observations projected onto KPCA1. Shaded bands mark the overlap region where k -means on KPCA1 alone cannot separate the two clusters.

The absence of nonlinear structure is itself a finding and closes the robustness critique: collinearity does not distort cluster geometry (Finding I), the data naturally supports three clusters but a six-cluster taxonomy is imposed (Finding II), and all six kernel functions—spanning distance-based (RBF, poly-2/3), information-geometric (Fisher–Mahalanobis), and graph-based (diffusion heat kernel) families—respect the six-cluster assignment in 2D. The airline profitability data harbour no hidden curvature.

4 Discussion

The Fisher Discriminant Analysis FDA requires pre-labelled membership; the research question requires structure discovery, making FDA circular. Statistically, with $n \approx 5$ – 9 per cluster, within-class covariance is near-singular, destabilizing the computation. FDA would be useful post-hoc

for sharper discriminant directions. Labelled data would also enable supervised manifold learning methods like linear discriminant analysis (LDA) or supervised kernel PCA, which could further validate the linearity finding by checking if supervised projections align with unsupervised ones.

The $ARI = 1.000$ finding (7D-raw vs 3D-PC) requires explanation. Collinearity stretches distance *along* the shared growth direction without reordering points *within* it. This dataset has chronological gradient encoded in PC1 (all variables grow monotonically 1995–2019 except crises). The six-cluster taxonomy partitions this gradient into six contiguous bands. Amplifying the growth axis by $\sim 3\times$ stretches all six bands proportionally—it does not reassign years across band boundaries, preserving clusters.

This invariance would *not* hold if clusters were orthogonal to the collinear direction. In a cross-sectional panel where low-cost and legacy carriers form clusters orthogonal to a time trend, collinearity would genuinely distort assignments.

The replication demonstrates robustness from three angles: (1) cluster assignments are invariant across spaces ($ARI = 1.000$), explained by temporal alignment; (2) 3D geometric visualization reveals the temporal band structure; and (3) kernel PCA across six kernels spanning three families (distance-based, information-geometric, graph-based) confirms the manifold is intrinsically linear, with cross-kernel agreement on the C_3 – C_5 ambiguous pair in 1D across all families. Together, these findings validate Renold’s headline claim that airline profitability regimes are stable across spaces.

5 Conclusion

This replication study validates the geometric robustness of Renold et al.’s airline profitability clustering while identifying critical gaps in methodological justification. The headline finding—that six-cluster structure persists when moving from raw 7D space to 3D-PC space ($ARI = 1.000$)—is confirmed through geometric visualization and kernel PCA validation. Collinearity, quantified by a participation ratio of 2.47, does not distort cluster assignments because the collinear direction (secular growth) is orthogonal to the partitioning criterion (temporal regimes). This orthogonality explains why amplifying the growth axis preserves clustering.

However, the silhouette criterion reveals a slight methodological tension: the data structurally supports three clusters, not six. The six-cluster solution is empirically defensible but statistically under-specified. Collinearity suppresses the silhouette signal that would surface $k = 3$ as the optimal choice. The recommended fix is straightforward: perform k -means on PCA score vectors (4D-PC space) rather than raw variables.

The cross-kernel validation via six independent kernel PCA implementations (RBF, polynomial, Fisher–Mahalanobis, diffusion heat) strengthens the conclusion: the airline profitability manifold is intrinsically linear. No hidden curvature exists, and all kernels preserve the six-cluster partition in 2D. This linearity finding, combined with temporal band structure visualization, closes the robustness critique and establishes that Renold et al.’s taxonomy is geometrically sound.

The paper’s headline claim that the airline profitability returns to pre-COVID patterns is empirically robust within the 1995–2020 observation window. The six-cluster taxonomy survives the collinearity critique intact: cluster assignments are invariant across all three spaces, 3D geometric visualization reveals the expected temporal band structure, and kernel PCA across six kernels spanning three families preserves the six-cluster partition in 2D. A cross-kernel 1D diagnostic provides additional confirmation.

However, silhouette evidence identifies only three natural regimes: low-profit (1995–2005), recovery (2006–2014), and peak-profit (2015–2019), with 2020 as a structural singularity. While the six-cluster solution is descriptively useful, collinearity ($PR \approx 2.47$) suppresses the silhouette signal that would otherwise surface $k = 3$ as the structurally motivated choice.

6 Future Work

Several directions merit further investigation:

Temporal dynamics and regime switching. The six-cluster taxonomy is stable across the 1995–2020 horizon, but the data exhibits punctuated transitions. A hidden Markov model or regime-switching vector autoregression could quantify state persistence and transition probabilities, moving beyond static clustering toward a dynamical system characterization.

Causal drivers of cluster membership. This replication examines the geometric structure but not the causal factors that induce transitions. Quantile regression or causal forest methods could identify which variables drive profitability regimes and whether collinearity masks causal signals.

Non-linear dimension reduction and manifold learning. This study validated the linear character of the airline manifold using kernel PCA across six kernels. Yet broader non-linear techniques such as t -distributed stochastic neighbor embedding (t -SNE), uniform manifold approximation and projection (UMAP), and autoencoders could reveal whether hidden nonlinear structure emerges under different topological assumptions or neighborhood metrics.

Generalization to other transport sectors. The participation ratio effect (2.47) may apply to public transport operator data, which often exhibit similar secular trends. A comparative study across sectors would test whether the collinearity–silhouette suppression pattern is transport-specific or domain-general.

7 Acknowledgments

The author thanks Prof. Renold for fruitful discussions and for making the data and methodology publicly accessible. The collaborative spirit of open science made this validation study possible. Thanks to Dr. Mayer for feedback on a draft version of this manuscript.

References

- [1] D. L. Davies and D. W. Bouldin. A cluster separation measure. *IEEE Transactions on Pattern Analysis and Machine Intelligence*, 1(2):224–227, 1979.
- [2] T. Hastie, R. Tibshirani, and J. Friedman. *The Elements of Statistical Learning: Data Mining, Inference, and Prediction*. Springer, New York, 2nd edition, 2009.
- [3] L. Hubert and P. Arabie. Comparing partitions. *Journal of Classification*, 2(1):193–218, December 1985.
- [4] J. M. Lyneis. System dynamics for market forecasting and structural analysis. *System Dynamics Review*, 16(1):3–25, 2000.
- [5] F. Pedregosa, G. Varoquaux, A. Gramfort, V. Michel, B. Thirion, O. Grisel, M. Blondel, P. Prettenhofer, R. Weiss, V. Dubourg, J. Vanderplas, A. Passos, D. Cournapeau, M. Brucher, M. Perrot, and É. Duchesnay. Scikit-learn: Machine learning in Python. *Journal of Machine Learning Research*, 12:2825–2830, 2011.
- [6] M. Renold, J. Vollenweider, N. Mijović, J. Kuljanin, and M. Kalić. Methodological framework for a deeper understanding of airline profit cycles in the context of disruptive exogenous impacts. *Journal of Air Transport Management*, 106:102305, January 2023.
- [7] P. J. Rousseeuw. Silhouettes: A graphical aid to the interpretation and validation of cluster analysis. *Journal of Computational and Applied Mathematics*, 20:53–65, 1987.
- [8] B. Schölkopf, A. Smola, and K.-R. Müller. Nonlinear component analysis as a kernel eigenvalue problem. *Neural Computation*, 10(5):1299–1319, July 1998.